Lunar Dust Characterization for Exploration Life Support Systems

Juan H. Agui *

NASA Glenn Research Center, Cleveland, 44135, USA

Lunar dust effects can have a significant impact on the performance and maintenance of future exploration life support systems. Filtration systems will be challenged by the additional loading from lunar dust, and mitigation technology and strategies have to be adapted to protect sensitive equipment. An initial characterization of lunar dust and simulants was undertaken. The data emphasize the irregular morphology of the dust particles and the frequency dependence of lunar dust layer detachment from shaken surfaces.

Nomenclature

a_s	Shaker table acceleration
A	Two dimensional (or cross-sectional) area
A_n	Fourier coefficients
C_c	Slip correction factor
D_s	Fractal Dimension
d_a	Aerodynamic diameter
d_e	Equivalent volume diameter
d_p	Particle diameter
F	Total or inertia ($= ma$) force
F_{adh}	Adhesion force
F_g	Gravity force
L	Length of profile
L_0	Roundness
L_n	Fourier descriptors
m	Mass
N	Number of steps
R	Radial distance
R_0	Equivalent radius
St	Stokes number
V	Velocity

Greek variables

χ	Shape factor
δ	Step size
μ	viscosity
ρ_p	Particle density
ρ_0	Standard density (1000 kg/m^3)
τ	Relaxation time
θ	Polar angle

*Aerospace Engineer, Microgravity Fluid Physics and Transport, AIAA Member.

I. Introduction

Future missions to the moon will have to contend with the ubiquitousness of lunar dust on the lunar surface. The pervasive nature of lunar dust will make it prohibitive to fully isolate all systems from its degrading and damaging effects, which can lead to an increased level of maintenance and mission risk. Numerous testimonials from the Apollo astronauts have emphasized the hazards of lunar dust with the strongest statement coming from John Young, Apollo 16 astronaut, who cautioned that "(Lunar) dust is the number one concern in returning to the moon."[1] In particular, the inhalation of lunar dust poses a serious biological hazard for the crew and the unique properties of these dust particles make it challenging to filter, capture, abate and maintain hardware under technologies designed for internal sources. Life support systems will have to be designed to handle these new challenges. In addition, long remote missions will demand and require that systems/subsystem elements be better designed for longer life, lower mass and regeneration.

In the past, particulate control for Space systems has received little attention. Recent data by Urban et al.[2] indicating that the particulate environment on the ISS is exceptionally clean (see Perry[3] for cleanliness requirements on the ISS) has attested to the high performance of the filtration system. In part, this could be attributed to the use of HEPA filters and the lack of any specific sources of significant particulate generation. To minimize sources most hardware systems and associated materials for use on the ISS are screened for maximum levels of offgasing and material degradation. However, with the longer duration missions and the possibility of additional particulate loading from the infiltration of lunar dust into the cabin or habitat, the importance of particulate control has to be more seriously considered.

To contend with the effects of lunar dust a more comprehensive understanding of lunar dust properties is essential to develop mitigation and control technologies for future robotic and manned missions. The seemingly most challenging features of lunar dust are its size and shape, toxicity and reactivity, abrasiveness, and adhesion properties. Studies here have begun to analyzed the shape properties of lunar dust particles through Fourier descriptors and fractal analysis. In addition, a preliminary experimental test was performed to assess the order of magnitude of the adhesion force between a layer of lunar simulant dust and a glass surface.

I.A. Background

The aerosol properties of suspended (airborne) particulate are most relevant in designing and assessing the performance of filtration systems. In particular, the size and shape of the particle plays a major role in the behavior of particulates in flow streams. It affects both the inertia and drag forces on the particle. These effects are best represented by Stokes number,

$$St = \frac{\tau V}{d_c} \tag{1}$$

and relaxation time,

$$\tau = \frac{\rho_p d_p^2 C_c}{18\mu} \tag{2}$$

V is the velocity of the flow stream , d_c is a characteristic size of the system or component (e.g. probe diameter), d_p is the particle diameter, C_c is the slip correction factor, and μ is the gas viscosity. d_p assumes a perfectly spherical particle which is rarely the case. The relaxation time relates to the time a particle takes to adjust its velocity (direction and magnitude) to new flow conditions or forces, and depends on particle and gas properties. For Stokes number, the velocity and characteristic size define the flow pattern, and the relaxation time gives an indication of the ability of the particle to follow the flow. For small Stokes number ($\ll 1$)the particles tend to easily follow the flow. For filters, this means that particles are able to penetrate fully through or through a certain thickness of the filter element. Particle shape is not very important in this case. However, for larger Stokes number, usually larger particles, the particles are readily intercepted by the filter element and the shape of the particle becomes important. Since most actual aerosol particles are irregular in nature, an aerodynamic diameter, d_a, is usually standardized for these calculations. It is defined as the diameter of an equivalent spherical particle with density of 1000 Kg/m^3 with the same settling velocity. To account for the irregularity of the particles, a shape factor, χ is usually used which is determined empirically for different shapes and types of particles typically by determining terminal velocities.

The relationship of the product of density and diameter squared can be shown to be,

$$\rho_0 d_a^2 = \frac{\rho_p d_e^2}{\chi} \tag{3}$$

d_e is the equivalent volume diameter and ρ_0, and ρ_p are the standard and particle densities respectively. d_a can readily obtained for this relation if the relevant particle properties and shape factor are known. Lunar particles are for the most part irregular particles having an average specific gravity of 3 g/cm^3, i.e $\rho_P/\rho_0 \approx 3$. In this case the aerodynamic diameter may over-predict the actual size of the particle. When it comes to the micron to submicron particle size range this size discrepancy becomes important. While filtration performance in based on aerodynamic particle size the toxicity is based on actual particle size and is most significant in the fine to ultrafine range. Therefore an assessment of the shape of lunar particles would be vital to inform both the filtration engineer and toxicologist.

Particle shape may also play a role in the adhesion of lunar particles to optical, thermal and sensitive surfaces, and fabrics including filter materials. There are several fundamental forces in determining the affinity of lunar particles to different types of surface materials at the molecular scale, but for larger particles the shape and surface morphology can also become important. The "hooky" shapes of agglutinates (discussed below) for example will tend to cling much easier to highly textured surfaces with asperities of the scale of the branched "hooks" on the agglutinates. The vesicles on agglutinates also may become lodged in the crevices on the surfaces. If the surface material is soft or pliable then the particles may become indented on the surface.

In reference to lunar dust particle size, the Lunar Source Book[4] and Graf[5] provide extensive lunar grain size data. Most of these measurements were performed through sieve studies and therefore the data was representative of the larger grain sizes (greater than a few microns). The statistical median of grain size ranged in value from 40 to 800 μ. More recent measurements by Greenberg[6] and Park et al.[7] have shown that the lunar regolith has a significant submicron content. Based on the method used, slightly different values were obtained, but both are indicative of fines below one micron. Both Greenberg and Park et al.'s recent data mark an important milestone in the analysis of the fines content of lunar regolith. However, more independent measurements are needed to provide more statistical confidence to the data.

It is also worth noting that the fractional gravity on the lunar surface may also affect the physics of lunar dust as an aerosol. Lower gravity levels lead to longer settling and interaction times and allow for the growth of aggregates. Aggregates are more massive and will tend to become more readily intercepted onto surface and pose different filtration requirements than individual particles. Also the very fine dust particles can be quite cohesive. This could also lead to the formation of large aggregates and may imply significant adhesion to surfaces.

Another important feature of lunar dust is its abrasive property. Forced air driven abrasive particle can abrade materials and surfaces reducing service life, an example being filter elements in an air ventilated cabin. Particle hardness, density, and again size and shape are significant factors in contributing to this effect.

Special focus on the morphology of lunar regolith particles is provided here.

I.B. Morphology

The Lunar Source Book provides several qualitative descriptors of lunar dust grains. These grains were characterized on average as being elongated, sub-angular to angular, and reentrant. Thus in general these particles are highly irregular and, as mentioned above, this property has several implications for life support systems.

Some of the lunar particles have quite unique morphologies. One particular example is agglutinates which are one of the more interesting and unique particles found in lunar regolith. They are aggregates of smaller lunar particles (mineral, grains, glasses and smaller agglutinates) bonded together by impact melted glass. Visually, agglutinates particles are quite roughened and irregular in shape. In some mature soils agglutinates are quite abundant making up as much as 60 % of the particles. To date no agglutinate like particles of natural formation have been found on earth. They are also not easily reproducible as a simulant.

For research and demonstration purposes the newest simulant, JSC-1a, is just now rolling out. It has been distributed in two main size classifications: root and fines. The fines being more relevant to investigation of dust properties and which been used in this study. An SEM of the JSC-1af is provided in figure 1. Individual particles were extracted from this micrograph for the shape analysis presented here.

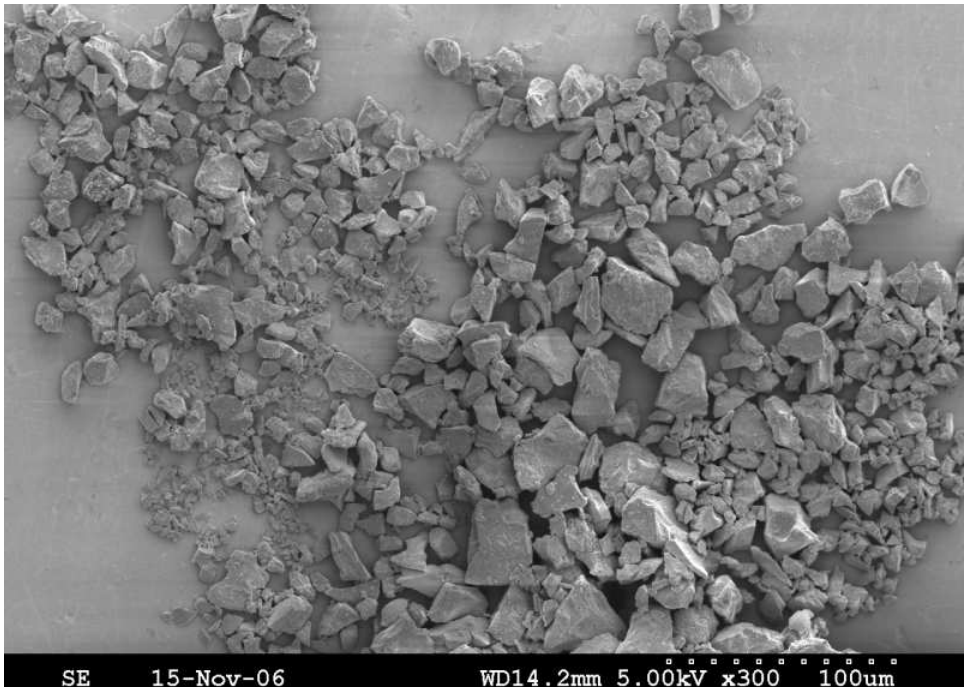

Figure 1. SEM micrograph of JSC-1a grains at 300X magnification. Courtesy of K. Street, NASA GRC.

Two digital analysis tools have been used to characterize and quantify, where possible, the morphology of lunar dust particles, agglutinates particles in this case, and simulant particles. The first is the use of Fourier descriptors which have been shown to yield several key characteristics of the overall particle shape as well as roughness. The second tool used was fractal analysis, which is used more for the study of aggregates but can also be used to study individual particle surface morphology. Agglutinates in particular are formed from the bonding together of smaller particles, as was explained, and are therefore well suited for fractal characterization.

I.B.1. Fourier Descriptors

Fourier descriptors have been used to analyze powders and grains (see references[8–10]). The particle profile is extracted from images of the particles and their coordinate points are found. The profile can be spatially decomposed into Fourier series components in either rectangular coordinates or by converting them into polar coordinates. A Fourier transform or decomposition is then performed. In the present case the polar coordinate Fourier decomposition was used. Therefore

$$R(\theta) = A_0 + \sum_{n=1}^{N} A_n e^{\mathbf{i}n\theta} \tag{4}$$

R and θ are the polar coordinate variables and A_0 and A_n are the Fourier coefficients of the transform. Several descriptors as given by Swanson[8] can be obtained from the transform coefficients. The first is the "equivalent radius",

$$R_0 = \sqrt{A_0^2 + \frac{1}{2}\sum_{n=1}^{N} A_n^2} \tag{5}$$

which would produce the same area/volume of an equivalent spherical particle. A measure of roundness can be found from,

$$L_0 = \frac{A_0}{R_0} \tag{6}$$

For irregular particles the term $1 - L_0^2$, also known as shape, is more appropriate. Thus the value of the shape term will increase with increased irregularity of the particle. The higher order terms provide additional shape tendencies,

$$L_n = \frac{1}{2}\frac{A_n^2}{R_0^2} \tag{7}$$

The lower order descriptors are related to the overall shape of the particles: L_0 is related to this size of the particle; L_2 to the elongation (ε) of the particle; L_3 to the triangularity (or triangular shape); L_4 to the squareness (or blocky shape). The summation of all higher order descriptor components provides a measure of the roughness of the particle. In general, the lower order descriptors are related to the larger scale angles while the higher order components better describe the smaller scale roughness of the particles. Thus, the increasing order descriptors represent larger and larger (tending towards flatter) physical angles.

The analysis consisted of extracting the rectangular coordinates from the profile of particle shapes using National Institute of Health's ImageJ software tools. A Scilab program was developed to transform the rectangular coordinates to polar coordinates and, using built-in functions, Fourier transforms were performed on the shape profiles. The Fourier descriptor were obtained by using the Fourier transform coefficients in the above relations.

I.B.2. Fractal Analysis

Most raw materials in nature are inherently fractal in character. Fractals are defined by their fractal dimension which quantifies the degree of self-similarity at different scales. At a basic level, a one dimensional line has a fractal dimension of one and a fully filled two dimensional area has a dimension of two. Therefore a two-dimensional fractal structure has a fractal dimension between one and two. Well known fractal structures are ferns, clouds, seashells. Fractals can also be quite instrumental in discerning particle aggregates since by their nature the overall shape is self-similar.

Fractals as a mathematical concept was popularized by Benoit B. Mandelbrot.[11] A fractal scaling law can be shown to follow,

$$N(\delta) \sim \frac{1}{\delta^{D_s}} \tag{8}$$

Here N is number of steps, of step size δ, needed to measure the length of the perimeter around a shape profile, and D_s is the fractal dimension. If the profile is fractal in nature N will be dependent on the step size, and will usually increase in length with decreasing step size, i.e. higher resolution measurement. A non-fractal profile will not change in length with higher resolution measurement. National Institute of Health's ImageJ software is a powerful image processing software used in a wide range of scientific fields. In this case we used the software to obtain the profile of particle shapes through various tools, and then invoked the FracLac plugin to conduct a standard box counting fractal analysis. FracLac outputs all relevant parameters.

Another method to establish fractal similarity or dimensionality of a set of objects is to establish the relationship in equation 9,

$$L(\delta) = C\delta^{(1-D)}\sqrt{A^{D_s}(\delta)} \tag{9}$$

This relationship has been used successfully to characterize the fractal dimensions of clouds.[12] The objects have to be fairly self-similar, i.e. a close in fractal dimension, in order to produce a relevant fractal dimension. ImageJ tools were used to extract the perimeter and area data from the shape profiles to perform the calculation.

II. Shaking Experiment

A shaking experiment was devised in order to obtain an indication of the adhesion force between a layer of dust particles and a surface. The equipment setup is shown in figure 2. The setup consisted of a sample cell, a VTS model 100 shaker, a piezo-electric accelerometer, a CCD camera, and all associated supporting electronics. The sample cell was composed of two glass slides with the dust layer deposited onto the bottom slide. Double sided adhesive tape was used as a gasket to seal and hold the slides together. The glass surface

was initially cleaned with alcohol and dried prior to the dust being sprinkled onto the surface. The glass surface was titled to remove and loosen any loose clumps of dust. This was performed several to ensure the best coverage of the imaging portion of the glass surface. A thin adhered layer composed of many islands or spots of dust remained behind. The cell was then mounted rigidly to the shaker table. The shaker (capable of up to 150 g's) was used to impart a vertical sinuousodal motion at different frequencies and amplitudes. A 20X long working distance objective was used for imaging.

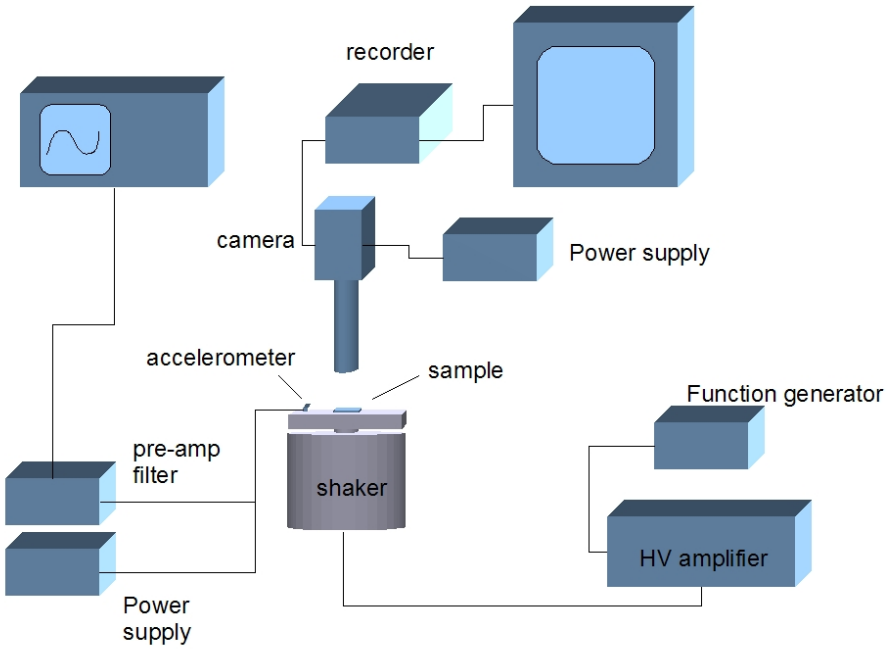

Figure 2. Setup of shaking experiment.

As the particles are shaken they experience the upward and downward acceleration of the upstrokes and downstrokes. When the acceleration amplitude is lower than earth's gravity then the particles fall with the downward moving surface. However when the acceleration amplitude is larger than g, the surface can move or accelerate sufficiently fast such that the falling particle can detach if it overcomes the adhesion with the surface. The forces involved are portrayed in figure 3. When the shaker table attains a negative acceleration which is $\geq g$, the force, F on the particles is,

$$F = F_g + F_{adh} \tag{10}$$

If the particle is still attached, the acceleration of the particle is the same as the acceleration of the shaker table, a_s. Then the adhesion force becomes,

$$F_{adh} = m(a_s - g) \quad for \;\; a_s \geq g \tag{11}$$

This suggests that there is no adhesion force when a_s is equal to normal gravity. When $a_s < g$ (i.e outside the range of validity) the particle is always held up by the shaker table. The maximum adhesion force is felt just before the particle separates from the surface. This is the force which is of engineering interest. To further refine this measurement knowledge of the particle contact surface area, or a model of it, is needed. This matter is quite complicated for irregular particles.

Initial tests were performed with commercial sandblasting glass beads of 120 grit (typically 120 μ). On close inspection the individual grains appear very spherical and they tended to easily roll around the glass surface upon slight tilting of the glass. The sample containing the glass beads was shaken at 100 Hz which was one of the frequencies used for the simulant experiment. The small fraction of the glass beads started to somewhat move around at an acceleration just below 1g. At an amplitude slightly above that of gravity (10.7 m/s^2) almost all the beads started dancing around the imaging plane.

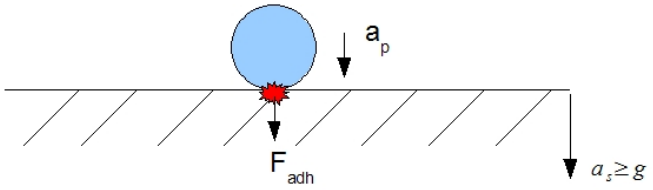

Figure 3. Shaking dynamics: Force diagram for $a_s \geq g$.

III. Results

The results of the main Fourier descriptors is presented in figure 4. A comparison of the magnitude of the Fourier components shows that elongation (or aspect ratio other than one) was the dominant mode. Relatively, the triangularity and squareness modes were significantly smaller components. However generally, the simulant particles did have somewhat elevated values of triangularity, L_3, over the regolith agglutinate particles and over the squareness mode, L_4. In fact, there was an isolated case of a simulant particle which appeared from visual inspection to be quite triangular and which gave a large of triangularity (see figure 4b). The elongation clearly appears to scale linearly with the shape of the particle. This is an indication that the more irregular the particle, the more likely the case that it is also elongated. Roughness was not significant for the simulant particles, but was somewhat pronounced for the agglutinate particles. Some agglutinate particles were several times higher in value.

A standard box count analysis was used to determine the fractal dimension of individual particles. Figure 5 shows a typical Richardson's plot of perimeter vs step size obtained through the box counting method. The fitting function shown in the plot is used to obtain the fractal dimension. In general, the simulant particles ranged in fractal dimension from 1 to 1.09, while the agglutinate particles were slightly higher in value ranging from 1.09 to 1.16. Clearly there is a distinction in fractal character between the simulant and agglutinate particles.

The Richardson (log-log) plot in figure 6 shows the relationship of equation 9 for the different particles analyzed. It shows two distinct slopes discriminating mainly between the simulant particles and the regolith agglutinate particles. A non-agglutinate regolith particle (provided by P.S. Greenberg, NASA GRC) obtained with high resolution SEM fell somewhere between the two trend lines. The fractal dimension obtained through this method was found to be slightly lower than the range of values found for individual particles through the more standard box counting method. This could be attributed to the set of fractal particles not being "similar" enough, in a fractal sense. In general, the data seem to indicate that the regolith agglutinate particles are slightly fractal in nature.

JSC-1af dust samples were tested on the shaker setup. Although the setup is currently in more of a feasibility phase, the preliminary data on the simulant sample shows that shaking could provide some mobility of the dust layer. It also indicates that the adhesion force was overcome by the aggregate layer of particles. Figure 7 shows snapshots before and after shaking of the dust layer. The marked region shows a distinct reshaping of the dust layer in this region. Upon close inspection other dust spots showed some movement or reshaping as well. This motion of the dust spots was noticeable at the higher frequency tested, 1000 Hz, and accelerations lower than that of gravity. This could be attributed to the presence of structural modes or a local resonant effect that augments the shaking. At the lower frequencies no noticeable motion

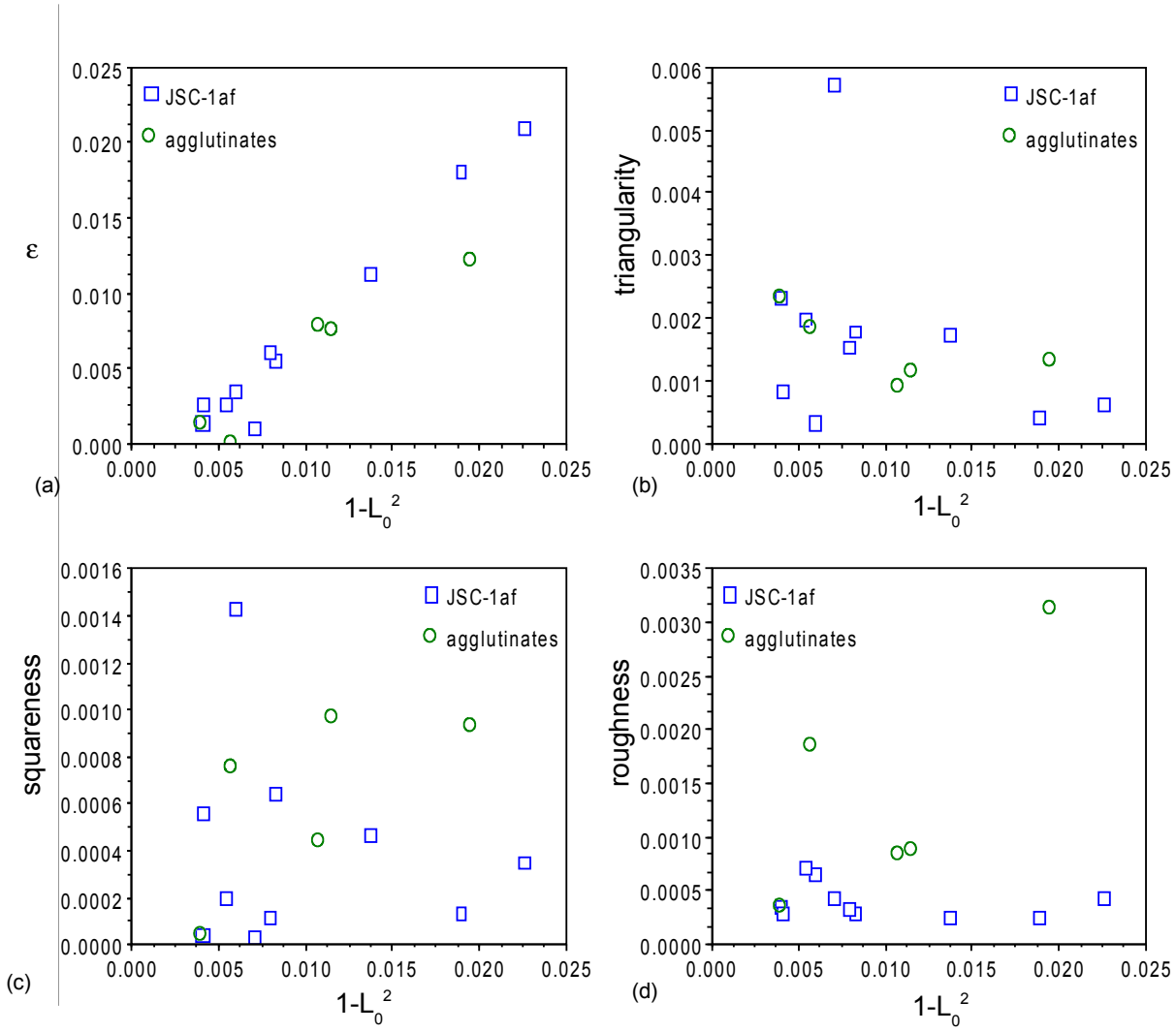

Figure 4. Fourier descriptors plotted against shape:(a)elongation, (b)triangularity, (c)squareness, and (d) roughness.

was detected even at very high acceleration amplitudes. More systematic testing is planned using this setup.

IV. Conclusion

Lunar dust effects can have a significant impact on the performance and maintenance of future exploration life support systems. In the past, little attention was paid to particulate control for Space systems. However, with the longer duration missions and the possibility of additional particulate loading from the infiltration of lunar dust into the cabin or habitat, the importance of particulate control has to be more seriously considered. The present data quantifies some of the morphological properties of lunar dust particles and JSC-1a simulant particles. Both the simulant and lunar regolith agglutinate particles were found to be more elongated. There was no dominant tendency towards an overall triangular or square (or blocky) shaped profile, although there was an individual case of high triangularity. Roughness was not significant for the simulant particles, but was somewhat pronounced for the agglutinate particles. The agglutinate particles tended to be slightly fractal in character. Finally, preliminary data on the shaking of dust layers on a glass surface showed that dust layer detachment occurred at higher frequency shaking. A model of contact surface area between the particles and the surface would be needed to develop this into an adhesion measurement at the particle layer. This is more easily done for the simulant particles then for the regolith agglutinate

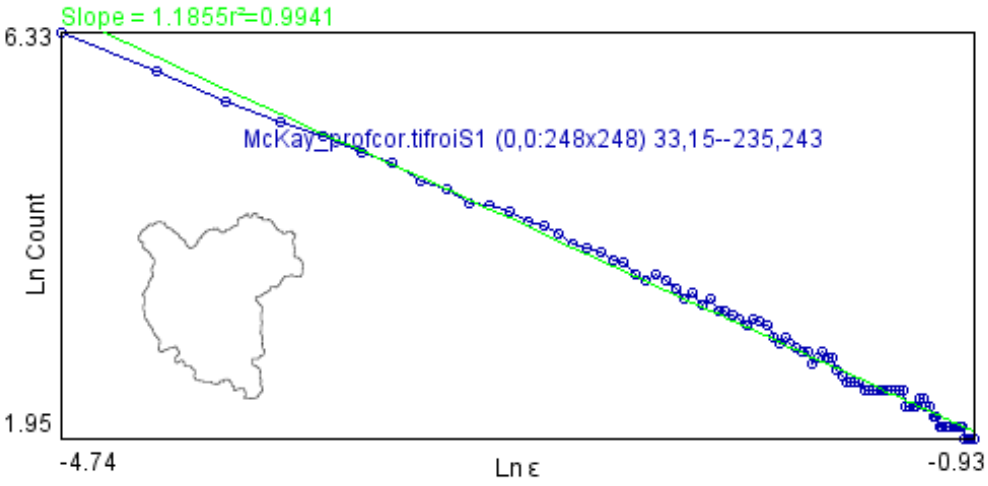

Figure 5. Richardson plot of length vs step size for an agglutinate particle (see inset of graph).

particles, which were found to have higher surface roughness and appeared to be more fractal in nature.

References

[1]D. Mackenzie. The gritty problem of moon dust. New Scientist, 28 May 2005.

[2]D. Urban, D. Griffin, G. Ruff, T Cleary, Jiann Yang, and G. Mulhollnad. Detection of smoke from microgravity fires. In *International Conference On Environmental Systems*. SAE, 2005.

[3]J.L. Perry. International space station bacteria filter element service life. NASA/TM 2005-213846, NASA, Marshall Space Flight Center, Alabama, 2005.

[4]B.M. French G.H. Heiken, D.T. Vaniman. *Lunar Source Book - A user's guide to the moon*. Cambridge University Press., 1991.

[5]J.C. Graf. Lunar soils grain size catalog. NASA/RP 1265, NASA, Washington, DC, 1993.

[6]P.S. Greenberg. Sensor development for the detection and characterization of lunar dust. In *Space Resources Roundtable VII: LEAG Conference on Lunar Exploration*, Houston, TX, 2005. SAE.

[7]J. Park, Y. Liu, K.D. Kihm, E. Hill, and L.A. Taylor. Submicron particle size distribution of apollo 11 lunar dust. In *ASCE Earth and Space 2006*, Houston, TX, 2006. SAE.

[8]P.A. Swanson and A.F. Vetter. The measurement of abrasive particle shape and its effect on wear. *ASLE Transactions*, 28(2):225–230, 1984.

[9]M.W. Clark. Quantitative shape analysis: a review. *Mathematical Geology*, 13(4):303–320, 1981.

[10]M.C. Thomas, R.J. Wiltshire, and A.T. Williams. The use of fourier descriptors in the classification of particle shape. *Sedimentology*, 42:635–645, 1995.

[11]B. B. Mandebrot. *The Fractal Geometry of Nature*, volume 27. W.H. Freeman, New York, 1982.

[12]S. Lovejoy. Area-perimeter relation for rain and cloud areas. *Science*, 216:185–187, 1982.

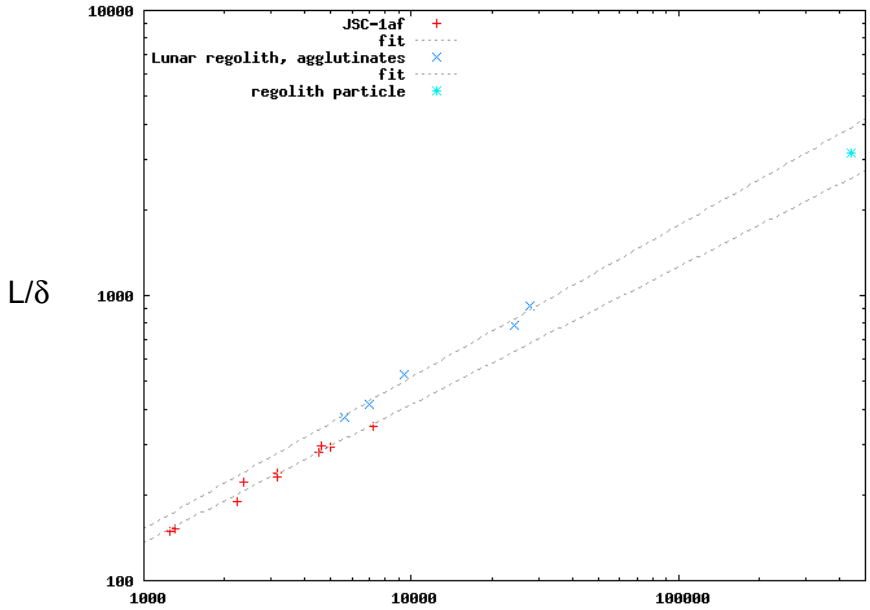

Figure 6. Richardson plot of length of perimeter vs area of the particles.

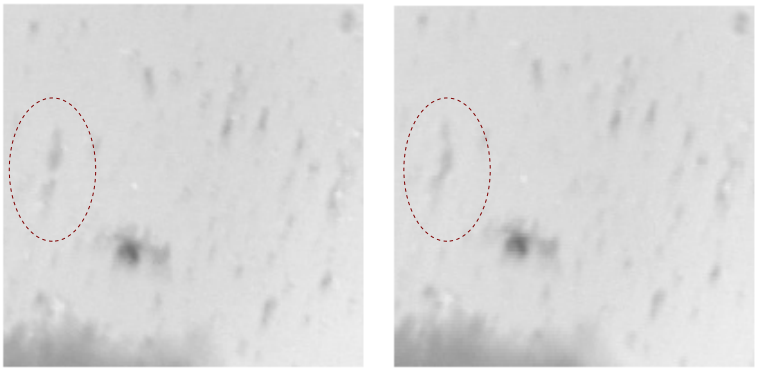

Figure 7. Close-up images taken of the shaken JSC-1a sample. The oval marked areas show a clear reshaping of the dust layer before and after shaking.